Pergamon

Int. J. Heat Mass Transfer. Vol. 40, No. 5, pp. 1017–1033, 1997
Copyright © 1996 Elsevier Science Ltd
Printed in Great Britain. All rights reserved
0017–9310/97 $17.00 + 0.00

PII: S0017–9310(96)00184–6

Contact angle temperature dependence for water droplets on practical aluminum surfaces

JOHN D. BERNARDIN, ISSAM MUDAWAR,† CHRISTOPHER B. WALSH‡ and ELIAS I. FRANSES‡

Boiling and Two-phase Flow Laboratory, School of Mechanical Engineering, Purdue University, West Lafayette, IN 47907, U.S.A.

(*Received* 2 *April* 1996 *and in final form* 20 *May* 1996)

Abstract—This paper presents an experimental investigation of the temperature dependence of the quasi-static advancing contact angle of water on an aluminum surface polished in accordance with surface preparation techniques commonly employed in boiling heat transfer studies. The surface, speculated to contain aluminum oxide and organic residue left behind from the polishing process, was characterized with scanning electron microscopy, surface contact profilometry, and ellipsometry. By utilizing a pressure vessel to raise the liquid saturation temperature, contact angles were measured with the sessile drop technique for surface temperatures ranging from 25 to 170°C and pressures from 101.3 to 827.4 kPa. Two distinct temperature-dependent regimes were observed. In the lower temperature regime, below 120°C, a relatively constant contact angle of 90° was observed. In the high temperature regime, above 120°C, the contact angle decreased in a fairly linear manner. Empirical correlations were developed to describe this behavior which emulated previous experimental data for nonmetallic surfaces as well as theoretical trends. Copyright © 1996 Elsevier Science Ltd.

1. INTRODUCTION

Relevance of surface wettability to heat transfer

The need to investigate the temperature dependence of the contact angle, θ, of water on aluminum in the present study stems from several boiling heat transfer investigations by the authors involving droplets. Previous experiments related to spray quenching of heat treatable aluminum alloys, revealed the importance of the wetting and spreading behavior of water droplets on high temperature surfaces [1, 2].

Aluminum is the most popular material in the aerospace industry because of its high strength-to-weight ratio and corrosion resistance. However, the processing of aluminum is plagued by product quality problems including surface cracking, nonuniform mechanical properties, and warping. One particular process which is largely responsible for these problems is the quenching of aluminum parts following solution heat treatment, casting, extruding, etc. Quenching involves exposing the high temperature part to a liquid quenchant such as water, resulting in a relatively large and rapid drop in the part temperature. Figure 1 displays a typical quench, or temperature–time cooling curve, for the surface of an aluminum part. At high surface temperatures corresponding to film boiling, the quench proceeds rather slowly as the liquid is separated from the surface by a continuous vapor blanket. As the surface temperature is decreased to the Leidenfrost point, the transition boiling regime is encountered where intermittent wetting of the surface begins and heat transfer rates increase with decreasing temperature. At a surface temperature corresponding to critical heat flux, most of the surface becomes available for wetting and intense nucleate boiling ensues, causing the part to cool rapidly until the quenchant's saturation temperature is reached, below which the part is cooled by single-phase liquid convection.

The present study was initiated to observe the temperature dependence of the contact angle of water on practical aluminum surfaces for the purpose of developing a better understanding of the influence of surface energy on boiling heat transfer between these two media. The contact angle is highly influenced by surface finish and the presence of impurities on the surface of both the liquid and solid. Table 1 highlights several studies on the contact angle of water on various metals [3–11]. In each study, various surface preparation techniques were used in attempts to obtain clean and homogeneous surfaces. Table 1 clearly indicates a wide spread in the contact angle data, which was speculated in many of the studies to result from contamination. It is apparent that even under highly controlled conditions, ideal surfaces are very difficult to produce and maintain. Moreover, it is extremely difficult and impractical to conduct boiling heat transfer experiments with perfectly clean and ideal surfaces such as those found in surface chemistry laboratories.

† Author to whom correspondence should be addressed.
‡ School of Chemical Engineering, Purdue University.

NOMENCLATURE

a	empirical constant in equation (1)
b	empirical constant in equation (1)
C	empirical constant in equation (1)
c_p	specific heat at constant pressure
d	thickness of surface layer in ellipsometry models
k	thermal conductivity, imaginary part of refractive index
N	complex refractive index $(n-ik)$
n	real part of refractive index
P	pressure
Ra	arithmetic average surface roughness
T	temperature
T_{co}	pseudo-critical temperature at which contact angle goes to zero
t	time
t_{eq}	duration of quasi-mechanical equilibrium regime
t_{ev}	duration of transient evaporation time
t_s	duration of transient spreading regime
x	coordinate along heated surface measured from drop center
y	distance perpendicular to heated surface
z	height of droplet interface above heated surface.

Greek symbols

α	thermal diffusivity
Δ	ellipsometry angle
θ	contact angle
λ_o	wavelength of light, in vacuum
ρ	density
σ	surface tension
Ψ	ellipsometry angle.

Subscripts

f	liquid
fg	difference between liquid and vapor
i	interface
o	initial
s	solid, surface
sf	difference between solid and liquid
sg	difference between solid and vapor.

It is well known that although metals are generally highly wetting, those found in practical devices such as heat exchangers, are commonly modified by system contaminants which drastically alter the surface wetting characteristics.

Thus, the surface condition for the present study was chosen to be similar to those found in boiling heat transfer studies where surfaces are mechanically polishing and then wiped with a volatile liquid. This procedure generally results in a surface containing polished paste residue, adsorbed impurities from laboratory air, and an oxide layer. While the absolute values of the contact angle measurements may indicate the presence of surface impurities, the present study of the temperature dependence of the contact angle is the first of its kind for high temperature water–metal systems. This study is intended to aid in explaining surface energy effects for practical laboratory prepared surfaces.

Fundamentals of wetting and spreading

The interaction of a liquid with a solid is referred to as wettability. When the liquid spreads spontaneously out as a thin film across the surface, it is said to 'wet' the surface. When the interactions are weak, the liquid beads up on the solid surface and the liquid partially wets the surface. The wetting characteristics of a vapor-liquid-solid system can be described by the interfacial energies (mJ m^{-2}) or tensions (mN m^{-1}). The interfacial tensions act in a direction tangential to the interface and arise from the nonisotropic nature of the pressure tensor at an interface [12]. The classical Young–Dupre equation, derived from a force balance parallel to the surface, of the interfacial forces at the intersection line of a vapor, liquid, and solid is given as

$$\sigma_{fg}\cos\theta = \sigma_{sg} - \sigma_{sf}. \quad (1)$$

Equation (1) can also be derived from a minimization of the total surface free energy which presumes thermal, mechanical, and chemical equilibrium. The Young–Dupre equation has several basic limitations. Firstly, while it effectively describes the force balance at the contact point, it is impractical since it is impossible to directly measure the solid–vapor and solid–liquid interfacial tensions, σ_{sg} and σ_{sf}, respectively. The two parameters which can be measured experimentally and are commonly used in describing surface wetting behavior are the equilibrium contact angle, θ, and the liquid–vapor surface tension, σ_{fg}, referred to as σ hereafter. Secondly, equation (1) assumes the solid surface is perfectly homogeneous, clean, and smooth; conditions which are rarely attainable in practical engineering situations. Finally, the interfacial tensions (at least the liquid–vapor tension) are those which apply far from the contact line. Adsorption of solutes or impurities, surface roughness, and near-contact line effects on the interfacial tensions have been explored by Dussan [13], Adamson [14] and Miller and Neogi [12].

The contact angle given in equation (1) is referred to as the equilibrium (ideal or hypothetical) contact angle which corresponds to a smooth, homogeneous, rigid, and isotropic surface with no fluid motion. Sev-

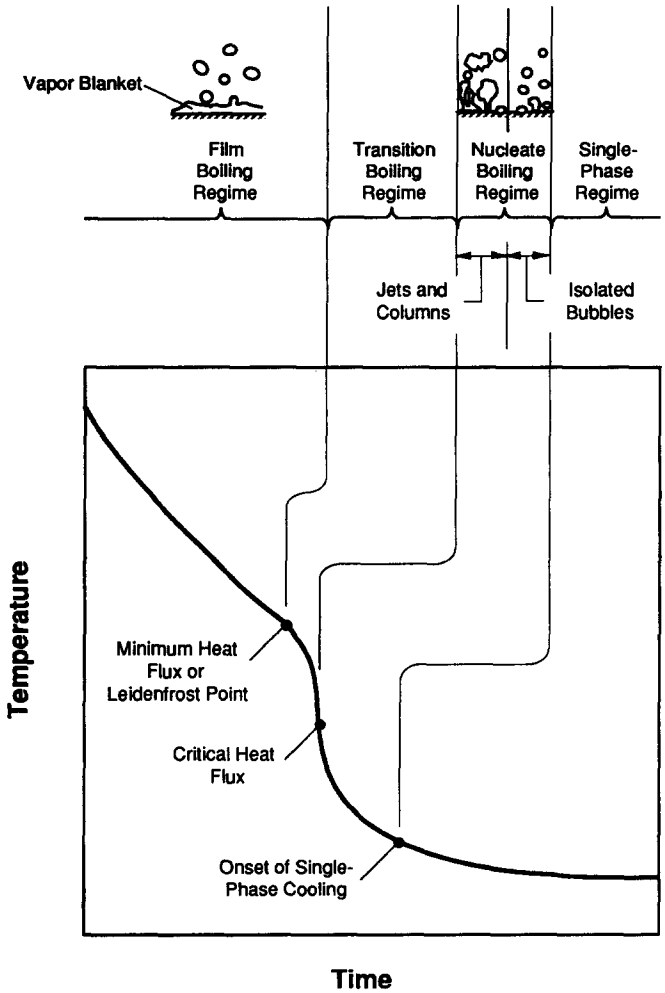

Fig. 1. Temperature–time history of a surface during quenching in a bath of liquid.

eral different contact angles commonly reported in the literature with conditions which deviate from this ideal behavior are summarized in Table 2. Each of these contact angles is defined by a unique set of conditions surrounding the interfacial system. The factors discussed above, fluid motion, and other non-equilibrium effects can significantly influence the contact angle and produce values which differ drastically from the equilibrium value [12–15].

The present work is concerned mostly with the quasi-static advancing contact angle which closely resembles the advancing contact angle most commonly reported in the literature. The fluid and thermal conditions leading to the definition of the quasi-static advancing contact angle are described in a later section. Other types of contact angle may also be relevant in boiling heat transfer but were not studied in detail because of dependence on material properties [16].

Surface chemistry and wettability play vital roles in many aspects of engineering and science including absorbency material development, waterproofing technology, and boiling heat transfer, to name a few. In particular, the contact angle and liquid/vapor surface tension influence boiling heat transfer through nucleation, growth rate, departure size, and departure frequency of bubbles [17–20]. Pool boiling studies by Diesselhorst *et al.* [21], Chowdhury and Winterton [22], Maracy and Winterton [23] and Unal *et al.* [24] revealed that critical and transition boiling heat fluxes are highly dependent on the wettability of the surface. Several important hypotheses and theories describing boiling regimes require knowledge of the contact angle behavior. For example, the smooth wall heterogeneous bubble nucleation theory, as reviewed by Carey [25], uses the contact angle to predict the superheat limit of liquids in smooth containers. In addition, Olek *et al.* [26] proposed the Leidenfrost point may correspond to a perfect wetting condition where the contact angle is zero.

Temperature dependence of contact angle

Several aspects which make it extremely difficult to relate the boiling process to the wetting characteristics

Table 1. Reported advancing contact angles of water on metal surfaces (some of which may contain surface oxides)

Reference	Surface	Surface preparation	Environment	Temp. [°C]	Contact angle [deg]
[3]	Gold	Pure metal wire surfaces dissolved prior to tests	Water vapor (2.8 kPa)	25	7
			Water vapor & pure air		6
			Water vapor & lab air		65
	Silver		Water vapor		10
			Water vapor & pure air		7
[4]	Aluminum	Various chemical cleaning methods followed by electropolishing	Water vapor at atmospheric pressure	25	4.6
	Brass				10.5
	Copper				9.6
	Magnesium				0
	Nickel				7.1
	Stainless steel				5.4
	Zinc				8.5
[5]	Gold	Commercial rolled	Water vapor at atmospheric pressure	101	85
	Silver	Heated to 600°C in H_2			85
		Plated on stainless steel			89
	Rhodium	Plated on silver			65
	Palladium	Polished, alumina			74
	Platinum	Polished, alumina			50
	Titanium	Polished, alumina			0
	Nickel	Plated on Cu–Ni			0
	Cadmium	Plated on Cu–Ni			0
[6]	Gold	Specimens heated to white-hot temperatures in various high purity gas streams	Pure gases at atmospheric pressure (hydrogen, krypton, neon, argon, nitrogen)	20	0
	Platinum				0
[7]	Gold	Alumina polished	Water vapor at atmospheric pressure	25	34–56
		Vacuum evaporated			62
		Diamond polished			61
		Film compressed			48–57
[8]	Gold	Mechanically and electro-polished	Helium	25	11–14
			Helium & water vapor	25	53
			Water vapor	101	63
[9]	Gold	Polished with MgO, rinsed, leached in HCl, rinsed, electrolytically degreased in NaCl, rinsed in distilled H_2O	Argon at atmospheric pressure	20	0
[10]	Gold	Polished with diamond paste, wiped with distilled H_2O, heated in O_2 and vacuum	Water vapor at atmospheric pressure	25	0–48
[11]	Copper	Sanded & polished with diamond paste degreased in mild detergent, rinsed: ethyl alcohol & distilled H_2O	Water vapor: 1.38 kPa	20.0	12
			Water vapor: 21.4 kPa	61.5	15
			Water vapor: 40.7 kPa	76.5	29
			Water vapor: 77.2 kPa	93.5	54
			Water vapor: 102.7 kPa	100.8	72

are the highly transient conditions associated with liquid–vapor phase change, the large temperature range encompassed by the various boiling regimes, and the lack of understanding of the temperature dependence of the contact angle. While a number of studies have been initiated to investigate contact angle temperature dependence for various liquids on non-metallic surfaces [14, 27–32], only a few investigations have been performed with water on metallic surfaces [21, 33]. Of course, surfaces of practical metals may not be metallic but contain an oxide or residue or both.

The temperature dependence of the contact angle is not well understood or documented, although it is reported to decrease with increasing temperature [25, 34]. Neumann *et al.* [29] and Adamson [35] reported that the temperature derivative of θ is negative with $|d\theta/dT| \approx 0.1$ deg K^{-1} for many systems at low tem-

Table 2. Definitions of contact angles

Contact angle	Schematic description	Definition
Equilibrium θ_e	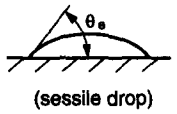	For thermodynamic equilibrium, this contact angle is given by Young's equation. This applies to an ideally smooth and homogeneous solid surface and a system free from contamination and fluid motion where the advancing and receding contact angles are equal.
Static advancing θ_a	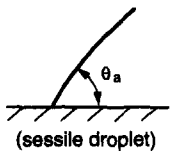	Contact angle obtained when liquid first advances and then comes to rest on an initially dry and clean solid surface.
Static receding θ_r	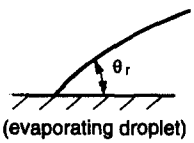	Contact angle obtained when liquid recedes and then comes to rest on a region of a solid surface which was previously occupied by the liquid (e.g. during evaporation with a moving contact line, or fluid removal with a fixed wetted area).
Apparent macroscopic θ_{ap}	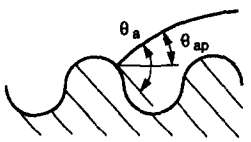	Contact angle formed by extrapolating the macroscopic liquid-vapor interface to the mean solid surface. Influenced by surface roughness, its value depends on the position of the contact line where the three interfaces intersect.
Microscopic θ_m	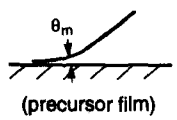	Actual equilibrium contact angle which exists in the microscopic precursor film in the near vicinity (<1 μm) of the apparent contact line.
Dynamic θ_d	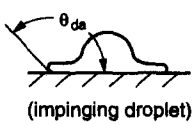	A non-equilibrium contact angle which exists during the dynamic spreading of the liquid on the solid surface. The liquid motion, caused by unbalanced surface tensions or external forces, can be advancing, θ_{da} or receding, θ_{dr}.
Quasi-static advancing θ_{sa}	See Fig. 6	The contact angle measured in this study which closely resembles the static advancing contact angle except for the following differences: the liquid droplet initially oscillates during surface collision and transient temperature and surface tension gradients exist in the droplet.

peratures (5–100°C). Petke and Ray [28] performed an extensive study of the temperature dependence of contact angle for water and several other liquids on six polymeric solids. They found $d\theta/dT$ for most cases to range from -0.03 to -0.18 deg K^{-1} over a temperature range of 5–100°C. They detected no systematic relationship between $d\theta/dT$ and the type of fluid or surface. In the surface temperature range of 100–160°C, $d\theta/dT$ decreased drastically for water on all six polymeric surfaces. For this high temperature regime, Petke and Ray reported that $d\theta/dT$ was negative and although values were not given, approximate values of -0.33–-1.17 deg K^{-1} could be inferred from the reported data.

While most of the studies on the temperature dependence of contact angle have been empirical in nature, a more fundamental study was presented by Adamson [35] in which a theoretical model related the molecular surface adsorption of a solid to the liquid–solid contact angle. Adamson used the Gibbs adsorption isotherm, thermodynamics, and a molecular interaction model to arrive at the following equation:

$$\cos\theta = 1 + C(T_{co} - T)^{a/(b-a)} \tag{2}$$

where T_{co} represents a pseudo-critical temperature, or the temperature at which the contact angle goes to zero, C is an integration constant, and a and b are temperature-independent constants from a balance of intermolecular forces. The model predicts the general experimental trends of θ with respect to T. For a few systems for which the contact angle has been observed to increase with temperature, Adamson suggested that this resulted from molecular interactions not accounted for in equation (2).

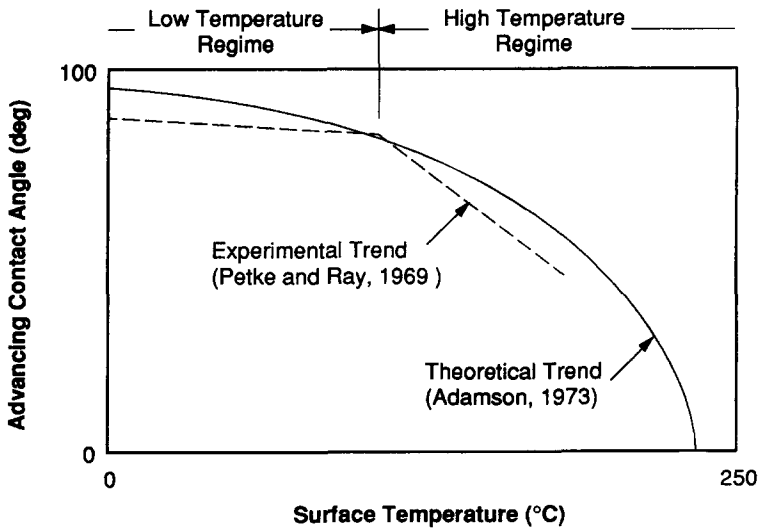

Fig. 2. Measured and theoretical trends of the advancing contact angle temperature dependence for water on an organic surface.

Figure 2 summarizes the general temperature-dependent trends for the contact angle of water on a polymer surface as found experimentally by Petke and Ray [28] and suggested theoretically by Adamson [35]. From the observed trends, two temperature regimes may be distinguished. In the low temperature regime, the contact angle varies slowly with temperature, having a gradient $d\theta/dT \approx -0.1$ deg K^{-1}. In the high temperature regime, the contact angle decreases more steeply with increasing temperature. Most investigations of the contact angle temperature dependence have focused on relatively low temperature ranges and practically no information exists for the high temperature regime [34]. Adamson [35], for example, was unable to provide high temperature contact angle data to verify the trend predicted by equation (2). In fact, the data used by Adamson to support his model appeared to lie along a straight line. Consequently, it is not known whether the limiting trend of the contact angle temperature dependence follows the linear relationship as suggested by existing experimental data for nonmetallic surfaces, or curves sharply as predicted by Adamson's theoretical model.

The above review points to two key observations which constitute the basis for the present study:

(1) Contact angle values employed by investigators in modelling boiling heat transfer from metallic surfaces can be quite erroneous since the true make-up of these surfaces can seldom be determined with certainty.

(2) The high temperature boiling regimes, for which the wetting character of liquids plays a paramount heat transfer role, are where few or no data are available for the contact angle temperature dependence for metallic surfaces.

By utilizing a pressure vessel to raise the water saturation temperature, the present study explores the contact angle dependence on surface temperature for temperatures as high as 170°C.

2. EXPERIMENTAL METHODS

Quasi-static advancing contact angles for water on a polished aluminum surface were determined using the sessile drop technique. Using a photograph of the droplet resting on the solid surface, the contact angle was determined by constructing a tangent to the droplet profile at the point of contact with the solid surface. This technique has the advantages of simplicity, reproducibility, and high degree of accuracy [14, 36].

Apparatus

The contact angle measurements were conducted in a 210 mm i.d. stainless steel pressure vessel illustrated in Fig. 3. Rated for 2.2 MPa at 220°C, this vessel enabled the measurement of contact angle at temperatures exceeding the boiling point corresponding to atmospheric pressure, in the absence of boiling and of rapid evaporation. The vessel's top flange contained ports for gas pressurization and liquid supply, a droplet catcher feed-through mechanism and both manual and safety relief values. The vessel possessed three side flanges, two were fitted with quartz windows for optical access (only one is shown in Fig. 3), while the third was used as a feed-through for electrical and instrumentation wires. Located within the pressure vessel was a droplet delivery system composed of a tubular liquid reservoir, a solenoid valve, a needle valve, and a hypodermic needle. The gas and liquid delivery lines were connected to a single compressed nitrogen tank. Two pressure regulators connected between the nitrogen tank and the pressure vessel allowed the liquid pressure to be maintained above that of the vessel. Using this pressurization technique,

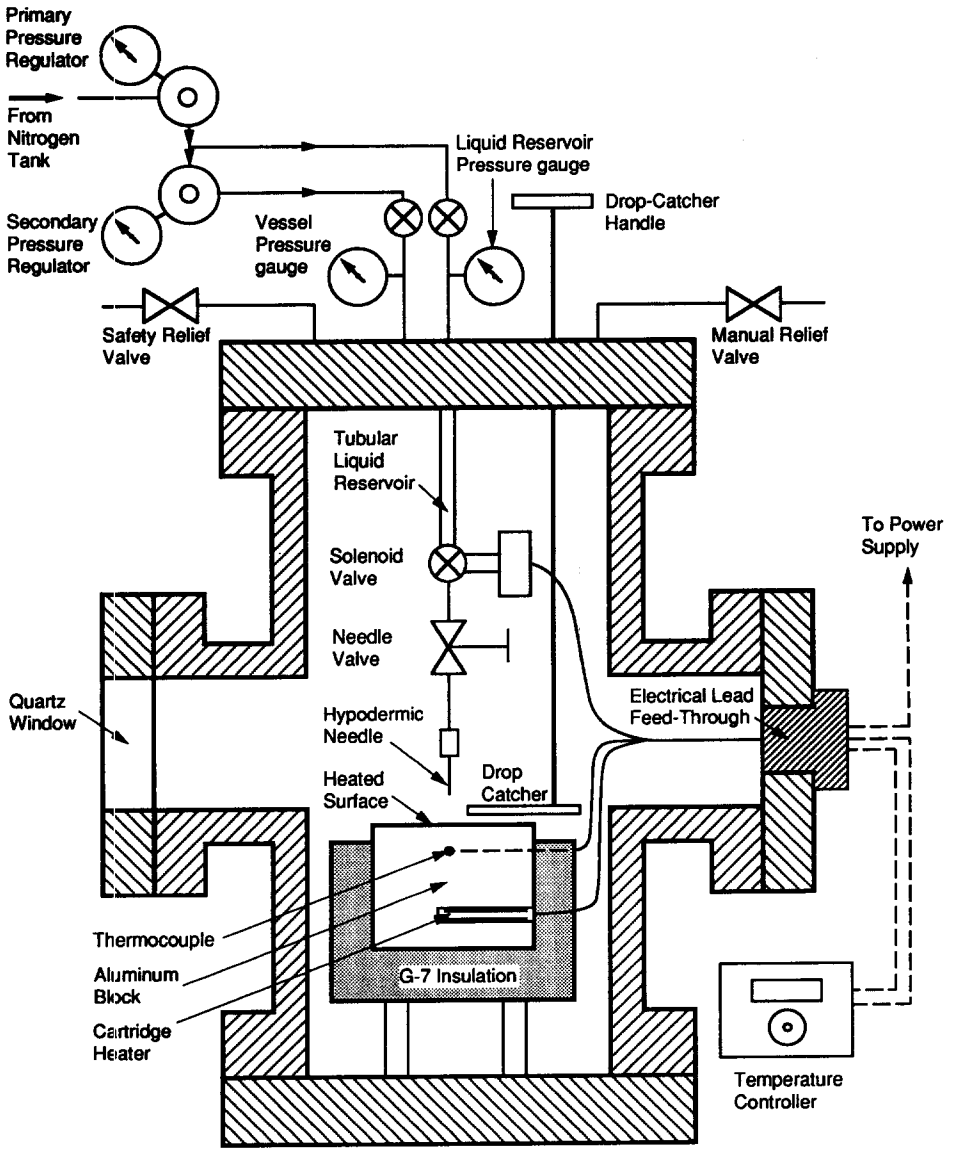

Fig. 3. Schematic diagram of pressure vessel used in contact angle measurements.

a liquid drop with an approximate diameter of 3.3 mm could be slowly formed at the end of the hypodermic needle and deposited onto the heated surface by opening and closing the solenoid valve. Distilled water was used throughout the experiments. The test surface consisted of an aluminum block which was heated by a 150 W cartridge heater. The surface temperature was monitored and controlled by an Ogden Type 33 temperature controller, which regulated electrical power input to the cartridge heater in response to a voltage signal from a chromel-alumel (type K) thermocouple located just beneath the center of the test surface. The vessel featured a manually operated drop catcher plate which shielded the heater surface from any additional drops once the desired drop had been deposited from the hypodermic needle.

A Nikon 35 mm camera, connected to a Questar QM1 long-distance microscope, and fitted with a Vivitar 283 electronic flash was used to capture photographs of the individual sessile drops from which the contact angle measurements were obtained.

Test surface characterization

The heater module was made from Al-1100, a 'commercially pure' aluminum with approximately 1.5% impurities made up of Mg, Cu, Si, Zn, Mn, and Fe [37]. The module was mounted in a G-7 insulating phenolic shell with its surface centered below the hypodermic needle as shown in Fig. 3. The heater module surface was initially sanded with 320 and 600 grit sandpaper, followed by additional sanding with Crocus cloth (3M product) and water. Finally, the surface was polished with Simichrome, an organic-based metal polish containing in part, ammonium oleate and aluminum and iron oxides. This surface preparation yielded a smooth, shiny surface with an arith-

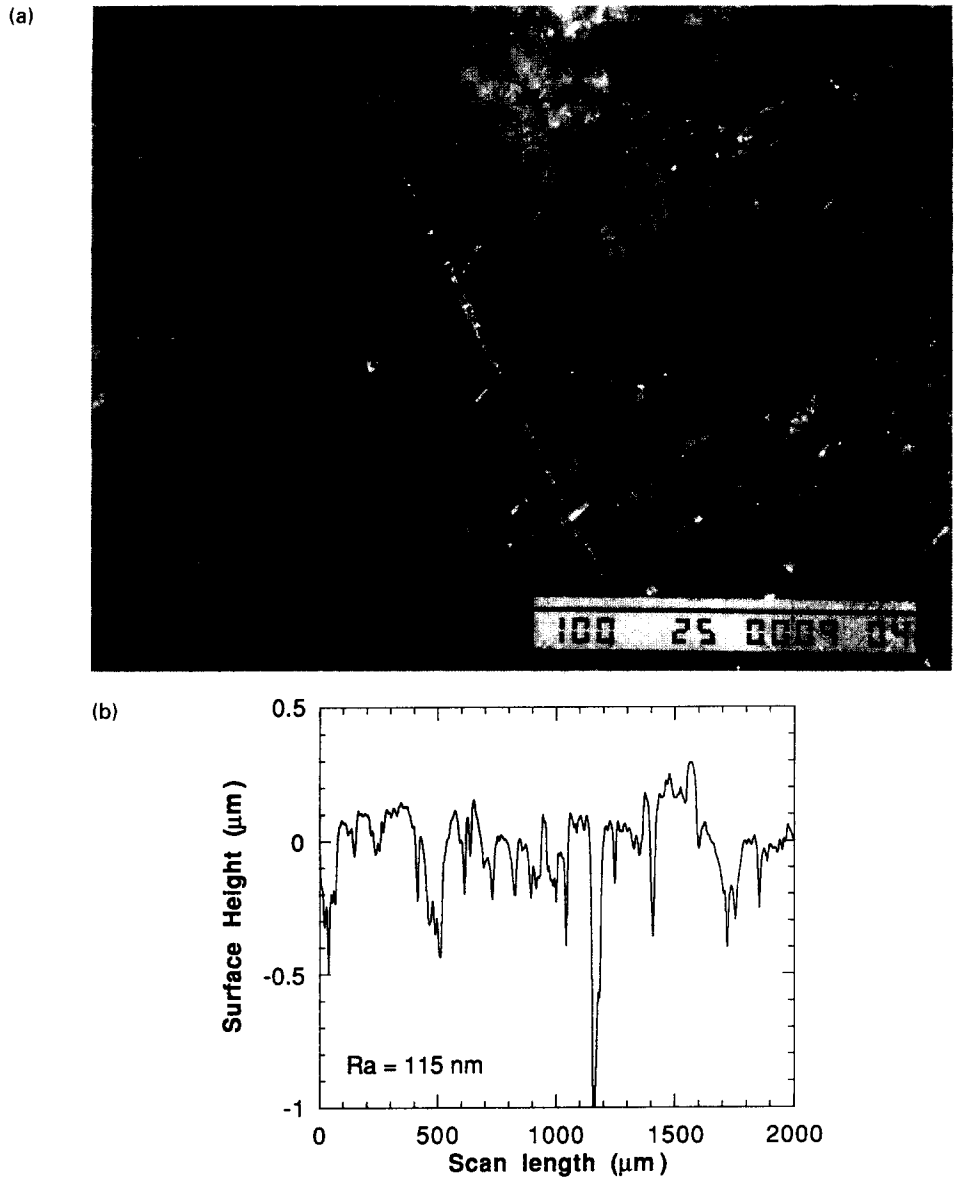

Fig. 4. (a) SEM image and (b) surface profile of the polished aluminum surface.

metic average surface roughness of 115 nm. This roughness value was determined from a surface profile obtained with an Alpha-Step 2000 contact profilometer and confirmed by scanning electron microscopy (SEM). Figure 4 shows an SEM image and a surface profile of the heated surface. The scale shown in Fig. 4(a) corresponds to 100 μm.

Since the wettability of a solid surface depends on both surface chemistry and roughness (as well as on certain dynamic conditions), it is important to characterize the influence of these factors adequately for the tested aluminum surface. Polished Al-1100 surfaces similar to the one employed in the present study were examined by Dardas [38] using X-ray photoelectron spectroscopy (XPS). He reported that all polished Al-1100 surfaces contain native Al_2O_3 with a thickness of 0.003 to 0.005 μm. Higher oxide thicknesses (0.01–0.04 μm) may be produced by heating above 750°C. Such oxides are substantially removed with the polishing procedure used.

The test surface was quite hydrophobic ($\theta = 90°$ at 22°C; see next section), perhaps as a result of some organic contaminant introduced by the polishing paste. Generally, absolutely pure aluminum surfaces should be hydrophillic (and high-energy) but are nearly impossible to produce because of the rapid formation of native oxide, which should also be hydrophillic. Hence, the material used here is neither pure aluminum nor pure Al_2O_3 on aluminum.

To characterize this surface further, ellipsometry measurements were performed in which the reflectivity of polarized light was observed [39]. In this technique, two angles, Δ and Ψ, are measured. Δ is related to the phase difference, and Ψ to the amplitude ratio of the

Table 3. Summary of ellipsometry results for polished aluminum Al-1100

Region†	ϕ (deg)	Δ (deg)	Ψ (deg)
A	70	126.77 ± 0.08	34.18 ± 0.03
B	70	127.1 ± 0.2	35.60 ± 0.04
C	70	127.5 ± 0.2	36.85 ± 0.03
A‡	70	128.2 ± 0.1	36.31 ± 0.08

† Region A (or B or C) represents an area of about 3 mm^2 at $\phi = 70$ deg.

‡ Sample was treated with methanol and measured again.

p- and *s*-polarized components of the reflected light. These two parameters are an overall measure of the complex refractive index, $N = n - ik$, thickness, d, of surface layer, and roughness of the aluminum substrate.

A Model L115 photometric ellipsometer from Gaertner Scientific Corporation with a He-Ne laser ($\lambda_o = 0.6328$ μm), a polarizer set at 45°, and a quarter wave plate (with fast axis perpendicular to the plane of incidence) were utilized. Three regions on the sample ($\approx 1 \times 3$ mm^2 each) were measured at an incident angle ϕ of 70° from the normal. Five consecutive measurements were taken in each region and averaged out. The results for Δ and Ψ are shown in Table 3 for three measurement locations, A, B and C.

While the ellipsometry measurements of Δ and Ψ effectively characterize the optical properties of the aluminum surface, they do not directly reveal the physical make-up of the surface. To investigate this make-up, several hypothetical surface models were assumed and the corresponding values of Δ and Ψ determined analytically. If the analytical values of Δ and Ψ from a hypothetical surface could be found to match the experimental values, then the possible structure of the surface can be identified. Various models were assumed and are discussed below. In each model, values of Δ and Ψ were determined for an incident angle, ϕ, of 70°, for several layer thicknesses and optical properties as displayed in Fig. 5(a) and (b).

For model 1, Fig. 5(a), $N = 1.43 - 7.48i$ was used to represent pure Al (the arithmetic average of two reported values by Palik [40]), for which $\Delta = 143.27°$ and $\Psi = 41.79°$ for $\phi = 70°$ (point P in Fig. 5(a)). These values are quite different from the observed data noted as A, B and C in Fig. 5(a), thus confirming the surface is not pure flat Al.

Also included in Fig. 5(a) is model 2, in which a flat Al_2O_3 layer ($N = 1.77$) on top of Al was assumed. In this model, the oxide layer thickness was gradually increased, creating the Δ and Ψ trajectory represented by the solid curve. Since the oxide is transparent ($k = 0$) for all realistic thicknesses, all calculated Ψ values fall far from the data. If an organic layer ($N = 1.45$) is placed on top of the Al_2O_3 layer ($d = 0.01$ mm of Al_2O_3, point Q) as indicated by model 3 in Fig. 5(a), the Δ and Ψ trajectory represented by the dashed line is obtained, which is also a poor representation of the data.

To better describe the data, model 4 was assumed with a partially absorbing material, with $N = 1.45 - ik$ of thickness d, and variable k and d. The value of $n = 1.45$ was chosen to represent organic material or aluminum. As shown in Figs 5(b), using Δ and Ψ at $\phi = 70°$, the data were predicted reasonably well with $k \approx 0.03$–0.06 and $d \approx 0.28$ μm. Small discrepancies can be related to surface roughness and surface chemical heterogeneity, both ignored in the model. Model 4 indicates that the surface layer is optically equivalent to a partially absorbing material on top of Al with a refractive index $N = 1.45 - 0.04i$ and $d \approx 0.28$ μm. The results do not imply that the actual surface layer is optically flat but suggest that it can be represented by a flat layer with equivalent optical properties, such as that described in model 4. The presence of surface roughness features in addition to various surface layers could produce a surface with similar optical properties. However, this would require a significantly more complex optical model in order to simulate the tested surface. Such a model is beyond the scope of this work, but warrants further study. The present results portray a practical aluminum surface which is more complex than pure aluminum oxide on top of aluminum, and point to a link to the wetting/spreading behavior to be discussed.

For the sake of completeness, the influence of polishing residue contamination was investigated using three different final surface preparations following the polishing process. In one set of experiments, the surface was left as-is following the polishing process. In a second set, the polishing was followed by soaking the surface for fifteen minutes in methanol and then wiping and rinsing with distilled water. In a third set, the heater module was heated in a nitrogen-atmosphere furnace to 475°C for 30 mins, then rinsed and wiped with methanol and distilled water.

Procedure

The contact angle measurements commenced by pressurizing the vessel and programming the temperature controller to the desired temperature. Three different pressures, 101.3, 524.0 and 838.3 kPa, and corresponding surface temperature ranges from 20 to 110, 150, and 170°C were investigated. Once steady-state conditions were reached, the solenoid valve was opened to dispense a single drop onto the heater surface, and then closed. Immediately following this step, the drop catcher plate was positioned beneath the hypodermic needle to prevent additional drops from falling upon the test surface. Five seconds after the placement of the drop, a photograph of the sessile drop was taken; reasons for this specific delay time will be discussed in the following section. Immediately after taking the photograph, the pressure vessel was depressurized and the heater surface manually repositioned so that a clean portion of the surface was located beneath the hypodermic needle for the next

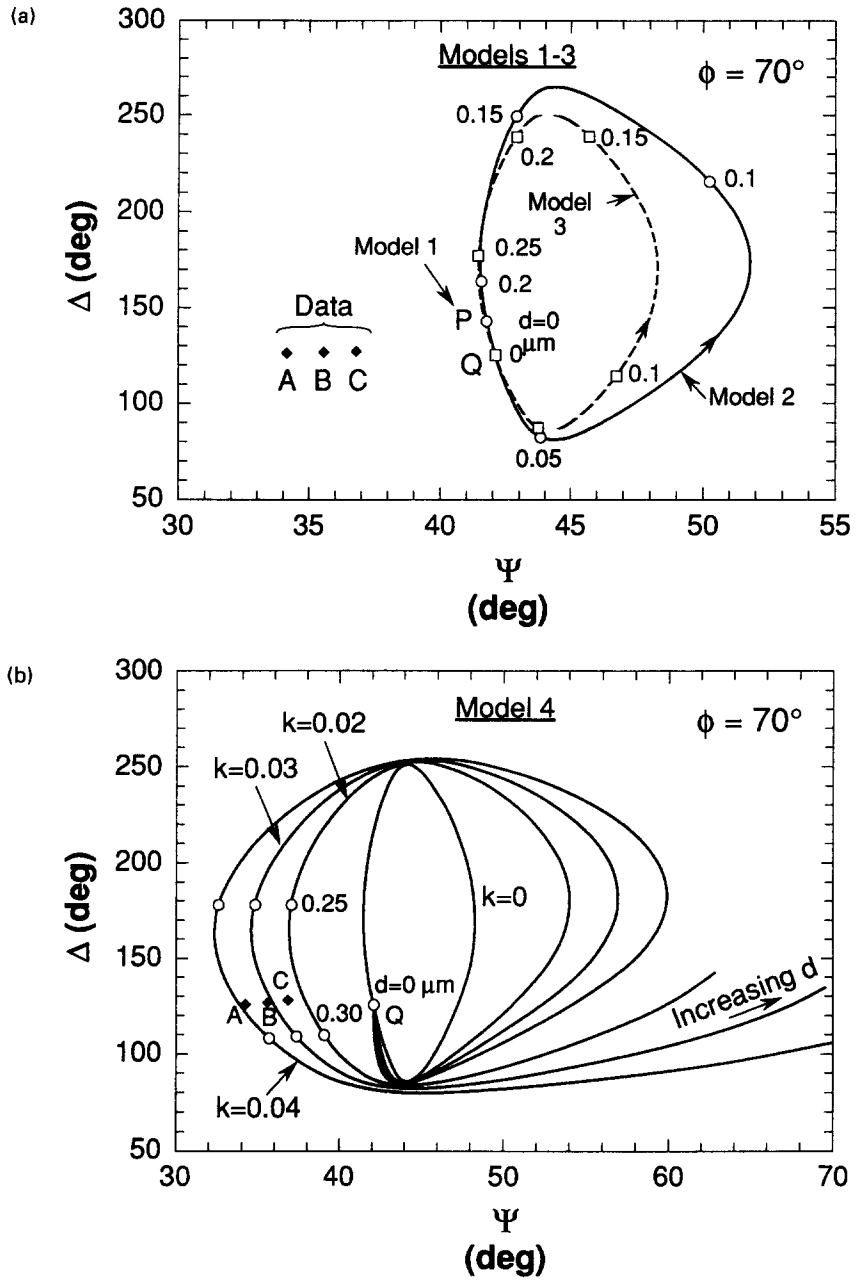

Fig. 5. Comparisons of Δ–Ψ data at three regions on the polished aluminum surface to calculated values for (a) model 1 (pure aluminum) or models 2 and 3 (transparent films) and (b) for model 4 (partially absorbing film on top of Al_2O_3) at $\phi = 70°$.

drop. Finally, contact angle measurements were made from the sessile drop photographs.

3. CONTACT ANGLE MEASUREMENT

The placement of a subcooled drop on the heated surface resulted in complex transient spreading and heating of the liquid upon contact. To obtain meaningful and reproducible data from the transient test conditions, the existence and extent of quasi-steady intervals had to be identified. High-speed photography and a mathematical model were used to observe and predict the drop spreading and heat transfer characteristics, respectively.

Figure 6 displays schematically the transient spreading radii and apparent contact angle of a droplet slowly being deposited on a surface from a falling height of 1 cm. During the initial period, or 'transient spreading regime', the droplet spread out upon the surface to form a thin film until reaching a maximum radius, after which it recoiled slightly and underwent several oscillations about a mean radius. During the initial spreading of the droplet, the contact angle at the leading edge of the film was large. This advancing

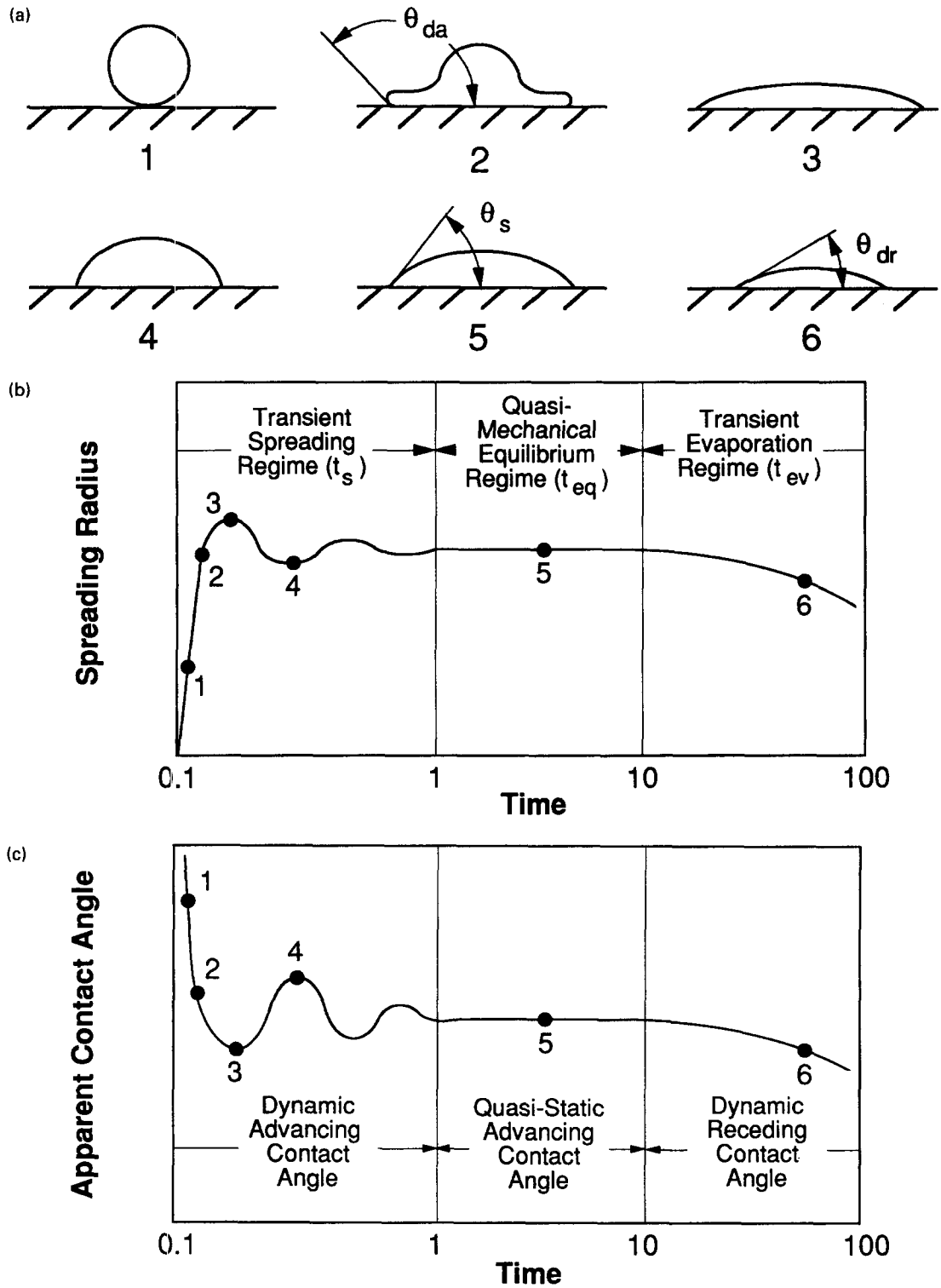

Fig. 6. (a) Qualitative sequential stages in the transient spreading of water droplet slowly deposited on a heated surface and the corresponding (b) spreading radius and (c) apparent contact angle. Times shown are only typical and vary according to temperature and pressure.

contact angle decreased continuously as the droplet reached its maximum extent and oscillated until a 'quasi-mechanical equilibrium regime' was established, as was previously suggested by Elliot and Ford [41]. The resulting quasi-static advancing contact angle was fairly constant during the quasi-mechanical equilibrium period while the liquid was heating up. At a later instant, the film entered a 'transient evap-

oration regime' during which the film receded and the contact angle continuously decreased.

High speed video results using a Kodak Ektapro 1000 motion analyzer revealed the transient spreading time of the droplet, t_s, was about 0.3 s. The extent of the quasi-mechanical equilibrium regime, t_{eq}, was dependent on pressure and surface temperature. For limiting conditions, t_{eq} was found experimentally to be as small as 5 s and as large as several minutes. The extent of the evaporation regime, t_{ev}, which followed the quasi-mechanical equilibrium regime, was highly temperature and pressure dependent. High speed video analysis and still photography both revealed that as heat was being rapidly conducted from the solid to the liquid–vapor interface, the contact angle decreased significantly from that in the quasi-mechanical equilibrium regime as the droplet began to evaporate, as expected for receding contact angles.

Figure 7 describes the transient heating experienced by the sessile drop under quasi-static mechanical equilibrium for three different interface temperatures. A one-dimensional, semi-infinite contact model [42] was used to estimate this transient temperature response for very short durations.

$$T_f(y,t) = T_i + (T_{f,o} - T_i)\,\mathrm{erf}\left(\frac{y}{2\sqrt{\alpha_f t}}\right) \tag{3}$$

where the constant interface temperature, T_i, between the surface and sessile drop is intermediate between the initial heater and fluid temperatures

$$T_i = \frac{(k\rho c_p)_s^{0.5} T_{s,o} + (k\rho c_p)_f^{0.5} T_{f,o}}{(k\rho c_p)_s^{0.5} + (k\rho c_p)_f^{0.5}}. \tag{4}$$

Liquid in close vicinity to the surface (<0.5 mm) dictates the wettability of the sessile drop. From the transient temperature model given in equation (3), the average surface temperatures in a liquid layer within 0.5 mm of the surface for various interface temperatures and times were determined, from which the average liquid surface tension was calculated using the relation [43]

$$\sigma = 75.83 - 0.15 T_f \tag{5}$$

where σ is expressed in mN m^{-1} and T_f in °C.

Calculations showed σ decreases from 72.5 mN m^{-1} at 22°C by roughly 20% over the first second following initial contact, but only by an additional 5% during the next 4 s. Thus, it appears transient heating may have a significant effect on contact angle measurements over only the first second of impact for the surface temperature range investigated.

Within the quasi-mechanical equilibrium regime, the droplet appeared stationary on high-speed video tape. However, transient heating of the droplet caused a transient nonuniform surface tension gradient to develop which in turn caused Marangoni flow [12] to occur along the droplet surface. This flow resulted in a slight distortion of the droplet profile. Figure 8(a) and (b) explore this effect by displaying both experimental and numerical sessile droplet profiles on a surface at temperatures of 22 and 150°C, respectively. The numerical profiles for the static interface are determined from the Young–Laplace equation and fluid hydrostatics [44]. By substituting geometrical relations for the principal radii of curvature of an axisymmetric droplet into the surface tension term of the Young–Laplace equation, a second order ordinary differential equation was obtained. This equation has been solved numerically by applying the proper boundary conditions to determine the droplet profile [44]. Figure 8(a) shows that the measured profile for $T_s = 22$°C closely matches the numerical predictions corresponding to a surface tension of 73.0 mN m^{-1}, thereby indicating the absence of impurities in the water. Figure 8(b), however, shows that the measured profile for $T_s = 150$°C is slightly distorted from the numerical predictions for two different surface tension values of 73.0 and 60.0 mN m^{-1}. Indeed, the measured profile cannot be described for this case by the Laplace–Young equation for any reasonable fixed value of surface tension. Hence, a surface tension gradient must exist and cause a substantial Marangoni surface stress, estimated to be about 5 N m^{-2}. Such a large stress should be more than adequate to cause significant Marangoni flow and droplet distortion.

Figure 9(a) displays the transient behavior of the contact angle at various instances of the sessile droplet lifetime for different surface temperatures and a pressure of 517.1 kPa. Figure 9(b) displays sequential photographs of the droplet lifetime for a surface temperature of 140°C. The variability of the contact angle with time made it necessary to select a consistent and meaningful time delay following impact at which the contact angle photographs were taken. A 5 s delay was determined from high speed video segments and the heat transfer model to correspond to a state of quasi-mechanical equilibrium and a constant solid–liquid interface temperature given by equation (4).

The effect of pressure on the liquid–vapor surface tension is expected to be relatively small for the pressure range used in this study because the liquid is nearly incompressible, and the intermolecular forces between liquid molecules do not change significantly. Thus, by sufficiently increasing the environmental pressure, the effect of surface temperature on the contact angle can be studied independently at temperatures well above the boiling point corresponding to atmospheric pressure.

4. CORRELATION OF CONTACT ANGLE TEMPERATURE DEPENDENCE

Figure 10 shows temperature dependent quasi-static advancing contact angle measurements for pressures of 101.3, 524.0 and 838.3 kPa. The relatively high values of the contact angle are expected not to result from Al or Al_2O_3, but from the presence of polishing paste residue on the oxidized aluminum test

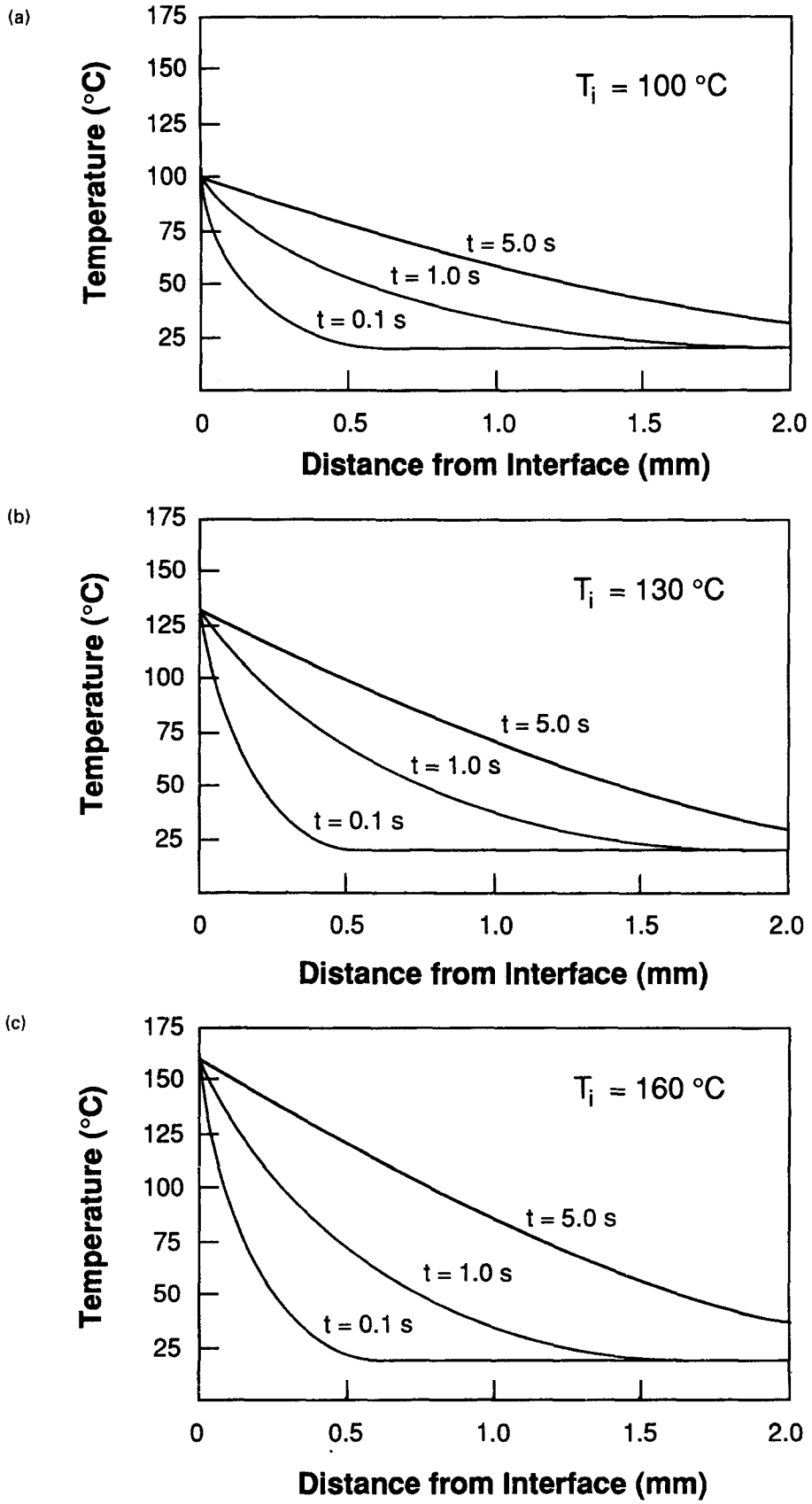

Fig. 7. Transient temperature profiles in a sessile drop for interface temperatures of (a) 100°C (b) 130°C and (c) 160°C.

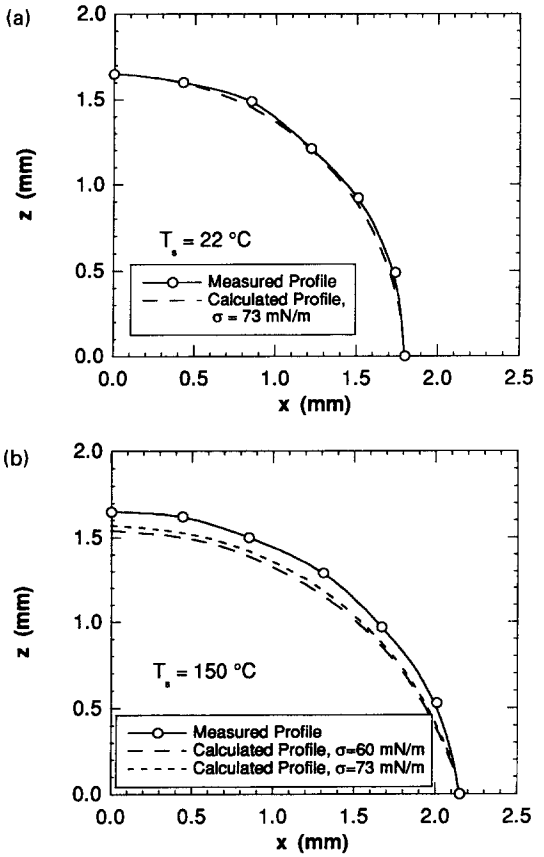

Fig. 8. Measured and calculated profiles for water drops for surface temperatures of (a) 22°C and (b) 150°C.

surface. As a comparison, Lai *et al.* [45] reported a contact angle of approximately 45° for water on alumina (Al_2O_3) at room temperature. The measured contact angle data show little variation with pressure and temperature for surface temperatures below 120°C. At surface temperatures above 120°C, the contact angle decreases fairly rapidly with increasing temperature. This temperature dependent contact angle trend is very similar to that reported by Petke and Ray [28] for water on six polymeric surfaces as discussed earlier.

Figure 11 displays contact angle measurements for three different tests in which attempts were made to remove any organic impurities possibly left behind from the polishing paste. In each case, the data exhibit the same general temperature dependent behavior displayed earlier in Fig. 10, but also indicate the presence of surface impurities even after attempted cleaning, as reflected in the high values of the contact angle and the larger scatter in the data. This is also consistent with the ellipsometry results. The scatter in the contact angle data is reflective of the data presented earlier in Table 1 in which reported contact angle values ranged from 0 to nearly 90° for water on extremely clean, high energy metallic surfaces. Even monolayers of organic impurities can cause large changes in the contact angle value of a pure system.

Figure 12 displays various curve fits, including linear, quadratic, and a polynomial form suggested by the theoretical model of Adamson [35] given in equation (2), for the data at 827.4 kPa. A constant contact angle of 90° was found to sufficiently fit the data for surface temperatures below 120°C, while linear and quadratic curve fits for surface temperatures above 120°C gave mean absolute errors of 1.6% and 12%, respectively. The linear extrapolation predicts that the contact angle goes to zero at $T_{co} = 286$°C, while the quadratic fit predicts a lower value of 226°C, as shown in Fig. 12(a) and (b), respectively. These two temperatures were substituted for T_{co} in a function similar to the theoretical form of equation (2) to arrive at the two curve fits displayed in Fig. 12(c). While these curve fits give reasonable mean absolute errors, the extrapolations at high and low surface temperatures do not appear to predict the contact angle temperature dependence as well as the linear and quadratic curve fits shown in Fig. 12(a)–(b).

The linear curve fit appears to provide the best approximation for both the low and high temperature ranges. This is the form most commonly reported for contact angle temperature dependence over low temperatures as previously discussed in the literature review. At high surface temperatures (>120°C), the contact angle appears to decrease linearly with increasing surface temperature. The trend proposed by the theoretical model of Adamson [35] appears to be in significant error for extrapolation to surface temperatures beyond those achieved experimentally in this study or by Petke and Ray [28]. It is, therefore, recommended that the following correlation be used for the temperature dependence of the quasi-static advancing contact angle of water on polished aluminum:

$$\theta = 90^\circ \quad T_s \leqslant 120^\circ\text{C}$$
$$\theta = 157.4 - 0.55T_s \quad T_s > 120^\circ\text{C} \qquad (6)$$

where θ and T_s are expressed in degrees and °C, respectively. While the magnitude of the contact angle is surface dependent, the results given in Fig. 11 suggest that the temperature dependence of the contact angle determined from equation (6) may be valid for other surface conditions as well.

5. CONCLUSIONS

The temperature dependence of the quasi-static advancing contact angle of water on a polished aluminum surface was investigated for surface temperatures ranging from 25 to 170°C and pressures from 101.3 to 827.4 kPa. Key findings from the study are as follows:

(1) Relatively high contact angles were measured for most experimental conditions. The hydrophobic nature of the surface is speculated to be the result of organic residue commonly left on surfaces following polishing processes.

(2) The contact angle of water drops deposited on a heated surface varies significantly over the drop

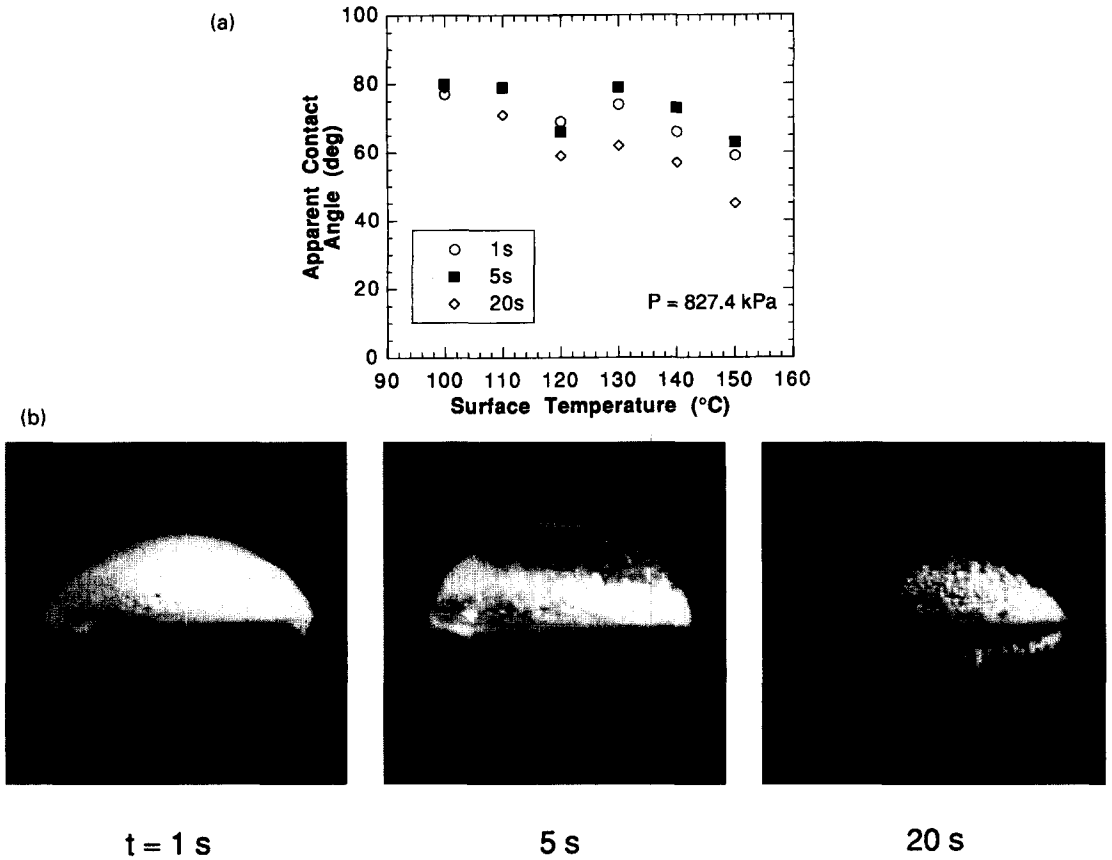

Fig. 9. (a) Temperature and time-dependent apparent contact angle measurements of sessile water drops on a polished aluminum surface at a pressure of 827.4 kPa and (b) photographic sequence of the droplet lifetime corresponding to a surface temperature of 140°C.

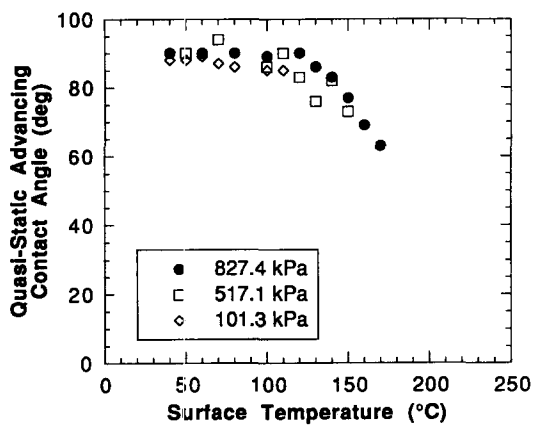

Fig. 10. Measured quasi-static advancing contact angle for water on polished aluminum for different temperatures and pressures.

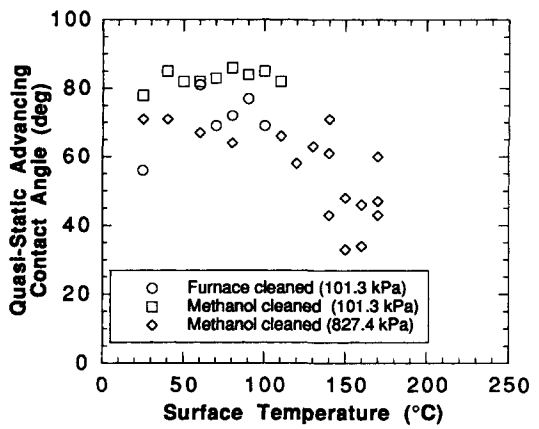

Fig. 11. Measured quasi-static advancing contact angle temperature dependence for water on a polished aluminum surface for various surface cleaning techniques.

lifetime. Three main regimes were identified, a transient spreading regime characterized by complex droplet oscillations and contact angle fluctuations, a quasi-mechanical equilibrium regime, where the contact angle is fairly constant, and a transient evaporation regime, where the contact angle gradually decreases due to evaporation. The quasi-mechanical equilibrium contact angle was found to resemble the advancing contact angle definition loosely adopted in the boiling heat transfer literature.

(3) While no pressure dependence for the contact angle was found, two distinct temperature-dependent regimes were observed. For surface temperatures smaller than 120°C a relatively constant contact angle of 90° was observed, and above 120°C the contact angle decreased towards zero.

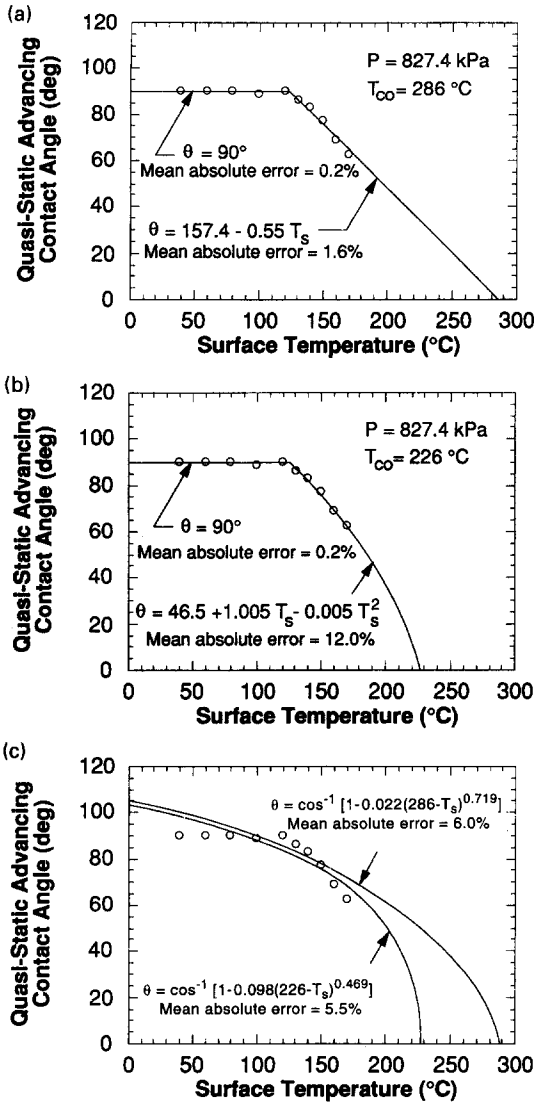

Fig. 12. Temperature-dependent quasi-static advancing contact angle correlation for water on a polished aluminum surface using (a) linear (b) linear/quadratic and (c) theoretical curve fits. All temperatures in the correlations are in °C.

(4) Empirical correlations were developed to describe the temperature dependence of the quasi-static advancing contact angle. These correlations reveal a dependence similar to that observed in previous experimental studies involving nonmetallic surfaces, as well as suggested by theory.

Acknowledgements—The authors thank Professor C. G. Takoudis for the use of his ellipsometer. The ellipsometry work was supported in part by NSF grant no. CTS 9311159.

REFERENCES

1. Bernardin, J. D., Intelligent heat treatment of aluminum alloys: material, surface roughness, and droplet-surface interaction characteristics. Masters Thesis, Purdue University, West Lafayette, IN, 1993.
2. Bernardin, J. D. and Mudawar, I., Validation of the quench factor technique in predicting hardness in heat treatable aluminum alloys. *International Journal of Heat & Mass Transfer*, 1995, **38**, 863–873.
3. Bartell, F. E. and Smith, J. T., Alteration of surface properties of gold and silver as indicated by contact angle measurements. *Journal of Physical Chemistry*, 1953, **57**, 165–172.
4. Trevoy, D. J. and Johnson, H. Jr., The water wettability of metal surfaces. *Journal of Physical Chemistry*, 1958, **62**, 833–837.
5. Erb, R. A., Wettability of metals under continuous condensing conditions. *Journal of Physical Chemistry*, 1965, **69**, 1306–1309.
6. Bewig, K. W. and Zisman, W. A., The wetting of gold and platinum by water. *Journal of Physical Chemistry*, 1965, **69**, 4238–4242.
7. White, M. L. and Drobek, J., The effect of residual abrasives on the wettability of polished gold surfaces. *Journal of Physical Chemistry*, 1966, **70**, 3432–3436.
8. Erb, R. A., The wettability of gold. *Journal of Physical Chemistry*, 1968, **72**, 2412–2417.
9. Bernett, M. K. and Zisman, W. A., Confirmation of spontaneous spreading by water on pure gold. *Journal of Physical Chemistry*, 1970, **74**, 2309–2312.
10. Schrader, M. E., Ultrahigh-vacuum techiques in the measurement of contact angles. II. Water on gold. *Journal of Physical Chemistry*, 1970, **74**, 2313–2317.
11. Boyes, A. P. and Ponter, A. B., Wettability of copper and polytetrafluoroethylene surfaces with water—the influence of environmental conditions. *Chemical Engineering Technology*, 1973, **45**, 1250–1256.
12. Miller, C. A. and Neogi, P., *Interfacial Phenomena*. Marcel Dekker, New York 1985.
13. Dussan, E. B. V., On the spreading of liquids on solid surfaces: static and dynamic contact lines. In *Annual Review of Fluid Mechanics*, Vol. 11, ed. M. Van Dyke, J. V. Wehausen and J. L. Lumley. Annual Reviews, Palo Alto, CA, 1979, pp. 371–400.
14. Adamson, A. W., *Physical Chemistry of Surfaces*. Wiley, New York, 1982.
15. Good, R. J., Contact angles and the surface free energy of solids. In *Surface and Colloid Science*, Vol. 11, ed. R. J. Good and R. R. Stromberg. Plenum Press, New York, 1979, pp. 1–29.
16. Berg, J. C., *Wettability*. Marcel Dekker, New York, 1993.
17. Hsu, Y. Y., On the size range of active nucleation cavities on a heating surface. *ASME Journal of Heat Transfer*, 1962, **84**, 207–213.
18. Han, C.-Y. and Griffith, P., The mechanism of heat transfer in nucleate pool boiling—Part I. *International Journal of Heat & Mass Transfer*, 1965, **8**, 887–904.
19. Johnson, M. A. Jr, De La Pena, J. and Mesler, R. B., Bubble shapes in nucleate boiling. *AIChE Journal*, 1966, **12**, 344–348.
20. Mikic, B. B. and Rohsenow, W. M., Bubble growth rates in non-uniform temperature field. In *Progress in Heat and Mass Transfer* Vol. 2, ed. T. F. Irvine Jr, W. E. Ibele, J. P. Hartnet. and R. J. Goldstein. Pergamon Press, New York, 1969, pp. 283–293.
21. Diesselhorst, T., Grigull, U. and Hahne, E., Hydrodynamic and surface effects on the peak heat flux in pool boiling. In *Heat Transfer in Boiling*, ed. E. Hahne and U. Grigull, Hemisphere, Washington, 1977, pp. 99–135.
22. Chowdhury, S. K. R. and Winterton, R. H. S., Surface effects in pool boiling. *International Journal of Heat & Mass Transfer*, 1985, **28**, 1881–1888.
23. Maracy, M. and Winterton, R. H. S., Hysteresis and contact angle effects in transition pool boiling of water. *International Journal of Heat & Mass Transfer*, 1988, **31**, 1443–1449.

24. Unal, C., Daw, V. and Nelson, R. A., Unifying the controlling mechanisms for the critical heat flux and quenching: the ability of liquid to contact the hot surface. *ASME Journal of Heat Transfer*, 1992, **114,** 972–982.
25. Carey, V. P., *Liquid–Vapor Phase Change Phenomena: an Introduction to the Thermophysics of Vaporization and Condensation Processes in Heat Transfer Equipment*. Hemisphere, New York, 1992.
26. Olek, S., Zvirin, Y. and Elias, E., The relation between the rewetting temperature and the liquid–solid contact angle. *International Journal of Heat & Mass Transfer*, 1988, **31,** 898–902.
27. Jones, J. B. and Adamson, A. W., Temperature dependence of contact angle and of interfacial free energies in the naphthalene–water–air system. *Journal of Physical Chemistry*, 1968, **72,** 646–650.
28. Petke, F. D. and Ray, B. R., Temperature dependence of contact angles of liquids on polymeric solids. *Journal of Colloid Interface Science*, 1969, **31,** 216–227.
29. Neumann, A. W., Haage, G. and Renzow, D., The temperature dependence of contact angles of polytetrafluoroethylene/*N*-alkanes. *Journal of Colloid Interface Science*, 1971, **35,** 379–385.
30. Tadros, M. E., Hu, P. and Adamson, A. W., Adsorption and contact angle studies I. Water on smooth carbon, linear polyethylene, and stearic acid-coated copper. *Journal of Colloid Interface Science*, 1974, **49,** 184–195.
31. Neumann, A. W., Harnoy, Y., Stanga, D. and Rapacchietta, A. V., Temperature dependence of contact angles on polyethylene terephthalate. In *Colloid and Interface Science* Vol. 3, ed. M. Kerker. Academic Press, New York, 1976, pp. 301–312.
32. Budziak, C., Vargha-Butler, E. I. and Neumann, A. W., Temperature dependence of contact angles on elastomers. *Journal of Applied Polymer Science*, 1991, **42,** 1959–1964.
33. Ponter, A. B. and Boyes, A. P., Wettability of copper and polytetrafluoroethylene surfaces with water—the influence of environmental conditions. *Chemical Engineering Technology*, 1973, **45,** 1250–1256.
34. Schonhorn, H., Dependence of contact angles on temperature: polar liquids on polypropylene. *Journal of Physical Chemistry*, 1966, **70,** 4086–4087.
35. Adamson, A. W., Potential distortion model for contact angle and spreading II. Temperature dependent effects. *Journal Colloid Interface Science*, 1973, **44,** 273–281.
36. Neumann, A. W. and Good, R. J., Techniques of measuring contact angles. In *Surface and Colloid Science*, Vol. 11, ed. R. J. Good and R. R. Stromberg. Plenum Press, New York, 1979, pp. 31–91.
37. Nock, J. A., Properties of commercial wrought alloys. In *Aluminum: Properties and Physical Metallurgy*, ed. J. E. Hatch. Americal Society of Metals, Metals Park, Ohio, 1984, p. 351.
38. Dardas, Z., XPS characterization of heat-treated aluminum alloys. Ph.D. thesis, Purdue University, West Lafayette, IN, 1993.
39. Azzam, R. M. A. and Bashara, N. M., *Ellipsometry and Polarized Light*. North Holland, Amsterdam, 1979.
40. Palik, E. D., *Handbook of Optical Constants of Solids*. Academic Press, Florida, 1985.
41. Elliott, T. A. and Ford, D. M., Dynamic contact angles, part 7—impact spreading of water drops in air and aqueous solution of surface active agents in vapor on smooth paraffin wax surfaces. *Journal of the Chemical Society, Faraday Transactions I*, 1972, **9,** 1814–1823.
42. Eckert, E. R. G. and Drake, R. M., *Analysis of Heat and Mass Transfer*. McGraw–Hill, New York, 1972.
43. Jasper, J. J., The surface tension of pure liquid compounds. *Journal of Physical Chemistry Reference Data*, 1972, **1,** 841–1010.
44. Hartland, S. and Hartley, R. W., *Axisymmetric Fluid-Liquid Interfaces*. Elsevier, New York, 1976.
45. Lai, C. L., Harwell, J. H., O'Rear, E. A., Komatsuzaki, S., Arai, J., Nakakawaji, T. and Ito, Y., Adsorption isotherms of perfluorocarbon surfactants from aqueous and non-aqueous solutions and friction measurements of perfluorosurfactant-adsorbed alumina. In *Colloid and Surfaces A: Physicochemical and Engineering Aspects*, Vol. 104. Elsevier, Amsterdam, 1995, pp. 231–241.